Changes in damaging hail in major Australian cities with global warming

Timothy H. Raupach[1,2,3], **Joanna Aldridge**[4,5]

[1]UNSW Institute for Climate Risk and Response, UNSW Sydney, New South Wales, Australia
[2]UNSW Climate Change Research Centre, UNSW Sydney, New South Wales, Australia
[3]ARC Centre of Excellence for Climate Extremes, Sydney, New South Wales, Australia
[4]School of Geosciences, University of Sydney, Sydney, New South Wales, Australia
[5]QBE Australia, Sydney, New South Wales, Australia

Key Points:

- **(Point 1)**
- **(Point 2)**
- **(Point 3)**

Corresponding author: Timothy H. Raupach, timothy.h.raupach@gmail.com

Abstract

(Abstract. . .)

Plain Language Summary

(Plain language summary. . .)

1 Introduction

Severe convective storms are responsible for insured losses of over $A40b in Australia from 1967 to 2023 (in 2022 dollars), accounting for 25% of insured catastrophe losses (Insurance Council of Australia, 2024). This includes the largest insured loss in Australian history: the April 1999 hailstorm impacting the eastern suburbs of Sydney, at $8.845b (in 2002 dollars, Insurance Council of Australia, 2024).

Insured losses due to severe convective storm are attributable to several hazards occurring within the same event: hail, extreme winds due to tornados, downbursts and straight-line winds, and extreme rainfall leading to water ingress and flash flooding. Typical severe convective storm catastrophe models generate synthetic event sets of hail and wind hazards as separate event footprints.

However, the coincidence of wind and hail is an important driver of loss. Wind-driven hail, both due to its greater force and oblique angle of impact, has greater potential to injure people, destroy crops (Changnon, 1967; Towery et al., 1976) and cause damage to the built environment, such as damaging cladding to external walls, smashing windows of buildings and motor vehicles and letting rainwater inside to damage internal fixtures and contents.

While wind loadings are currently considered in the Australian building code (Australian Building Codes Board, 2024) under standard AS1170.2 (Standards Australia, 2021), the impact of hail and wind-driven hail is not currently considered in Australian building design. The Association of Consulting Structural Engineers (2022) discuss hail loading on roofs and acknowledge that this effect is not accounted for under the current design standards. The April 2015 hail event impacting western Sydney is discussed including the collapse of warehouse buildings from hail loading on roofs. A guide of ultimate limit and service limit state designs for various building types is presented, but wind driven hail is not considered. Some roofing products are tested for hail impacts against standards, but many products are unrated.

In ICC building code (International Code Council, 2008), hail is considered in two hail regions in the USA defined using observational data: moderate and severe, depending on the likelihood of at least one day of 1.5 mm **(o2)** 3 mm hail in a 20-year period. This code requires testing of roofing materials such as asphalt, wood and slate shingle, clay or concrete tiles, metal roofing panels and shingles in these zones. The changing occurrence of hail over time is not considered. In Canada, while hail impact is not considered in the current building code, although change is being sought in the aftermath of the 2020 Calgary hailstorm which caused $C1.4b of insured loss. Resilience measures may include increasing roof slope, using resistant roofing materials and roof underlays (Institute for Catastrophic Loss Reduction, 2018). They found that a steeper roof limits damage from wind-driven hail on the leeward side. The lack of research into impact resistant non-roof housing elements, such as windows, doors, sidings, fascia and skylights, is noted, and these elements are often subject to damage in the most destructive storms.

This study seeks to understand how the coincidence of extreme winds and damaging giant hail (> 5 cm) may change in a future climate. Severe thunderstorms are convective systems defined by the Australian Bureau of Meteorology to be accompanied at least one of the following:

- Hailstones with a diameter of 2 cm or more
- Wind gusts of 90 km/h or greater
- Flash flooding
- Tornadoes

Wind driven hail events are defined as hail exceeding 5 cm and wind gusts exceeding 100 km/h (27.8 m/s) occurring in the same system within a 1 hour timeframe. Wind driven hail events are most likely to be associated with supercells where downbursts occur.

(Previous studies to include:)

- (Allen et al., 2014) used an environment-based approach to suggest an increase in severe thunderstorm incidence in south-east Australia, although with a wide range of uncertainty.
- (Walsh et al., 2016) review the current and future storm-related wind and hail hazard in Australia and found future projections of wind hazard increase along the populated east coast of Australia.
- (Carletta, 2010) identified that squall lines and isolated cells and clusters of cells as the most frequent systems associated with wind driven hail for the USA using observational data.
- (Bell et al., 2023) has compiled 1646 hail and wind damage swaths for the mid west of the USA using MODIS satellite observations for use in future understanding of the frequency of these events.

2 Methods

2.1 Simulations of historical and projected weather

Historical and future simulations were produced using the Advanced Research Weather Research and Forecasting (AR-WRF) weather model version 4.4.1 (Skamarock et al., 2021) for four nested domains covering major Australian cities. We used one coarse- (∼27 km grid spacing), two medium- (∼9 km), and four fine-resolution (∼3 km) domains with a parent-child scaling ratio of three. The model domains are shown in Figure 1 and parameterisation schemes used are shown in Table 1. WRF-HAILCAST (Adams-Selin et al., 2019) was enabled for the fine-resolution domains, to estimate maximum hailstone diameters at the surface. Boundary condition inputs were prepared using the `nc2wrf` code of Xu et al. (2021a).

Table 1. Parameterisation schemes used in the WRF simulations.

Microphysics	P3-3moment (Milbrandt et al., 2021)
Cumulous (medium and coarse nests only)	New Tiedtke (Zhang & Wang, 2017)
Longwave and shortwave radiation	RRTMG (Iacono et al., 2008)
Planetary boundary layer	YSU (Hong et al., 2006)
Surface layer	Revised MM5 (Jiménez et al., 2012)
Land surface	Noah-MP (Niu et al., 2011)

Simulations were run for two scenarios of 20 convective seasons each: the historical scenario ran from 1989 to 2009, and the future scenario from 2080 to 2100. For each convective season, simulations were run from 00Z September 30 to 18Z February 28, with hourly output resolution. Outputs were converted to local summer time and subset to cover October 1 to February 28 inclusive in each season. For each season the 14–16 simulated hours on 30 September local time were discarded as model spin-up time. Model outputs

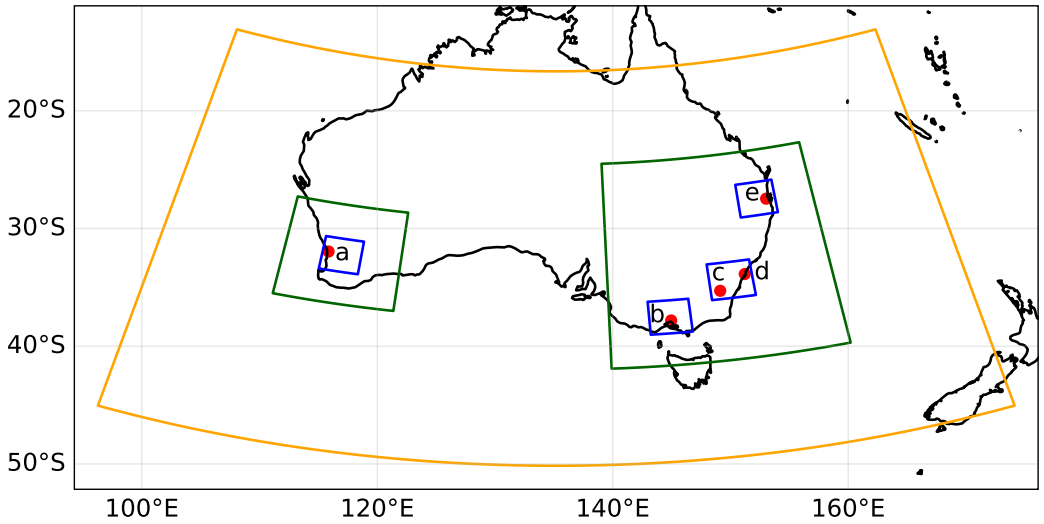

Figure 1. Approximate extents of the model domains on a map of Australia. The coarse-resolution domain is in yellow, medium-resolution domains in dark green, and fine-resolution domains in blue. Approximate city locations (with city extents not shown) are marked with red points for a) Perth, b) Melbourne, c) Canberra, d) Sydney, and e) Brisbane.

provide instantaneous values – that is, the values at each hour – for most variables, including wind speed at 10 m. In contrast, for each grid point and each hour, HAILCAST outputs the maximum hail diameter over all model timesteps during the previous hour.

The timestep for the coarse domain was set to 100 s, but reduced to 80 s or 60 s for simulation days on which Courant-Friedrichs-Lewy (CFL) errors occurred **(see comment in Section 4; this implies that hailcast was run more often on some days than others but the difference should be small because we use the daily maximum hail size over the whole domain)**.

2.2 Data preprocessing

Examination of maximum hail size fields showed that HAILCAST had a tendency to produce occasional unreasonably large hail sizes, particularly over ocean areas. Since our focus is on hail hazard on land, we therefore subset the data to land areas using WRF land mask with small holes filled and a slight erosion applied so that points over the coean, large bodies of water, or on the coastal boundary are not considered in this study. Further, we removed from consideration any HAILCAST value of surface hail over 180 mm diameter. HAILCAST has been updated in more recent versions of WRF than used here, and while the updated version reduces the occurrence of unrealisatically large hail sizes the changes do not affect the majority of HAILCAST results, meaning that removing very large hail sizes as we do here leaves a reasonable dataset for analysis (pers. comm. B. Adams-Selin, 2024). In all, between **(X)**% to **(X)**% of all hail diameter values were removed, depending on the domain.

2.3 Statistical modelling of extreme values

Modelling of extreme values was done using the R (R Core Team, 2023) package `extRemes` (Gilleland & Katz, 2016). Block maxima were defined as daily maximum hailstone size per domain, under the assumption that such a timeseries would be close to independent

(Coles, 2001) given that a single hail storm would never last more than one day. We used quantile-quantile (QQ) plots (Coles, 2001) and the Kolmogorov–Smirnov (KS) test to assess the goodness of fit of the GEV models. The KS test was used to assess the match between the empirical distributions and values drawn from the fitted GEV models. For each model, 1000 values were drawn from the GEV and compared to the empirical distribution; this process was repeated 100 times for each distribution.

3 Data

Boundary conditions used for the simulations were bias-corrected data for downscaling by Xu et al. (2021b). These boundary conditions have a mean climate and interannual variance derived from European Centre for Medium-Range Weather Forecasts Reanalysis 5 (ERA5, Hersbach et al., 2020), with a non-linear trend derived from the ensemble mean of 18 Coupled Model Intercomparison Project Phase 6 (CMIP6, Eyring et al., 2016) models (Xu et al., 2021b). Future projections used the "middle-of-the-road" SSP2-4.5 shared socioeconomic pathway (SSP, O'Neill et al., 2017).

4 Results

4.1 GEV analysis and goodness of fit

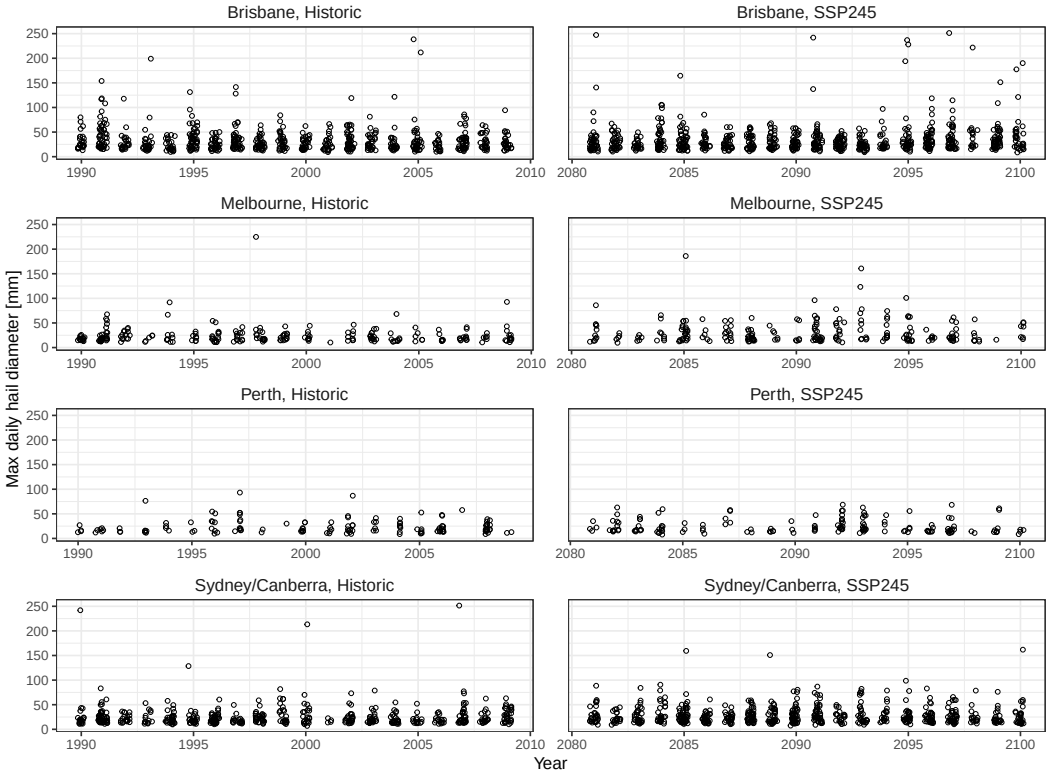

Figure 2. Time series of daily maximum hail sizes by domain and epoch.

Figures 2 and 3 show timeseries of daily maximum hail sizes and 10 m wind speeds, respectively. GEV models were fitted to each of these datasets. Figure 4 and 5 show QQ plots for the hail size and wind speed distributions, respectively. The QQ plots for wind speed show excellent agreement between the model and empirical quantiles. The QQ plots

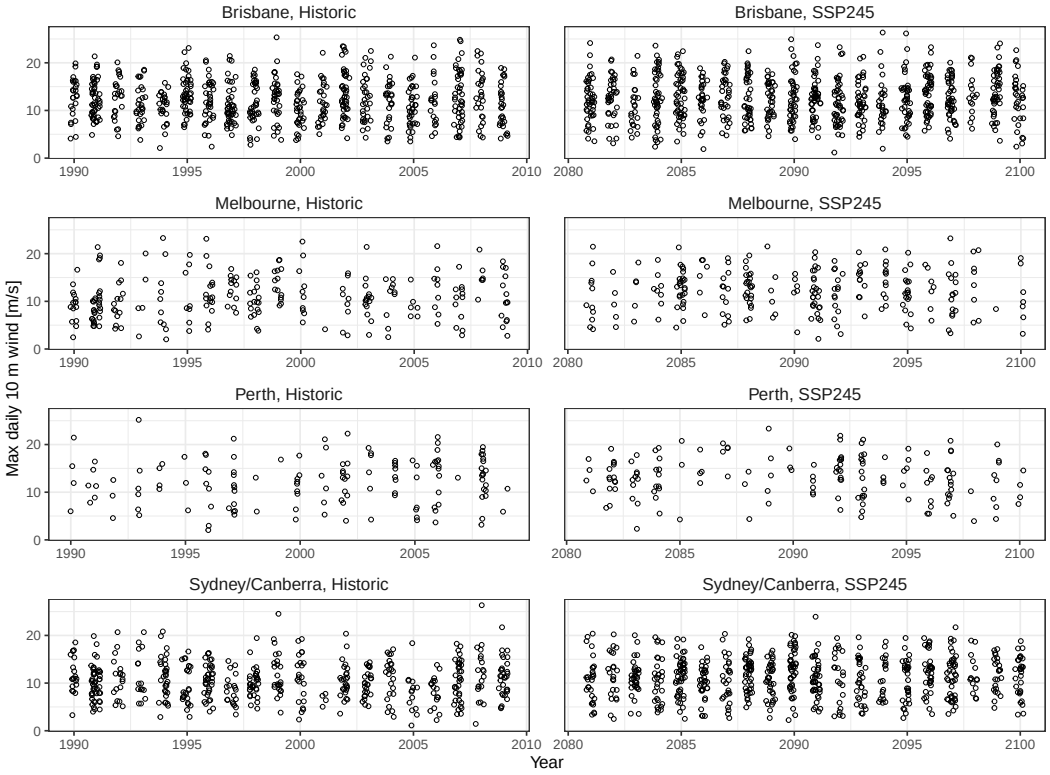

Figure 3. Time series of daily maximum 10 m wind collocated with hail.

for hail size show an acceptable agreement with some model overestimation of high quantiles. The distributions of resulting p values from the KS test are shown in Figure 6. In all cases where the model was compared to empirical values, either all or the bulk of p values are above the 0.05 level, indicating that the null hypothesis that the two samples are drawn from the same distribution can not be rejected. We take the QQ plot and KS test results as an indication that the GEV fits are sufficient for the analyses we show here.

Having determined that the GEV fits are valid, we now consider whether the fitted models show any significant difference between the historical and future periods considered. Figure 7 shows the fitted parameters and their confidence intervals for all the GEV models used in this study. The models fitted for the Melbourne and Sydney/Canberra domains both show significant differences in parameters between the historical and SSP245 scenarios, whereas the models for Brisbane and Perth domains have parameters with overlapping confidence intervals. These results are echoed by the p value distribhihisutions from KS tests (Figure 6) when historical model is compared to the SSP245 model. For maximum hail size, the null hypothesis that the samples are drawn from the same distribution can be rejected for the Melbourne and Sydney/Canberra domains, while for 10 m wind this null hypothesis can be rejected for Melbourne, Perth, and Sydney/Canberra. To be conservative, we conclude that the changes between epochs are significant in the Melbourne and Sydney/Canberra domains, but not significant in Brisbane and Perth.

4.2 Changes in hailstorm frequency

- **(Include changes in variability in annual hailstorm frequency.)**

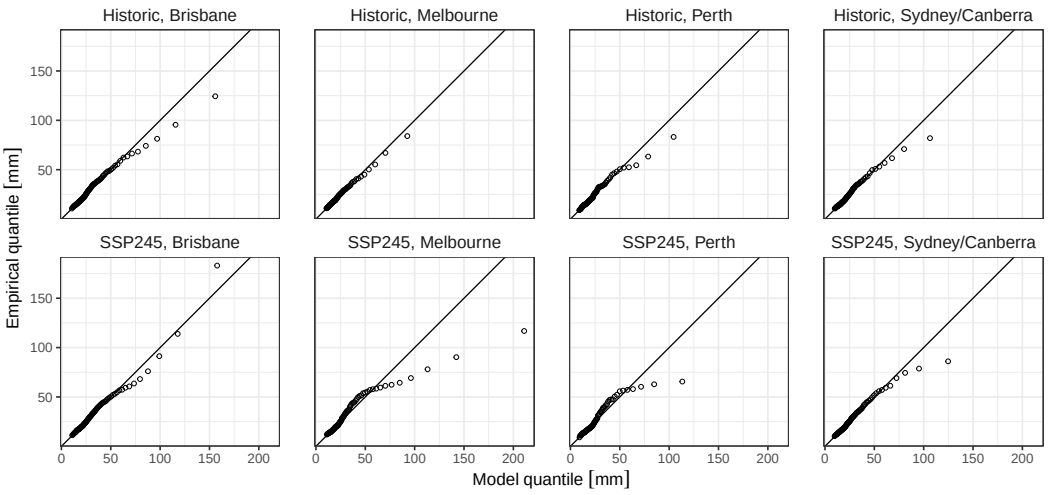

Figure 4. Quantile-quantile plots for GEV models fitted to daily maximum hail sizes.

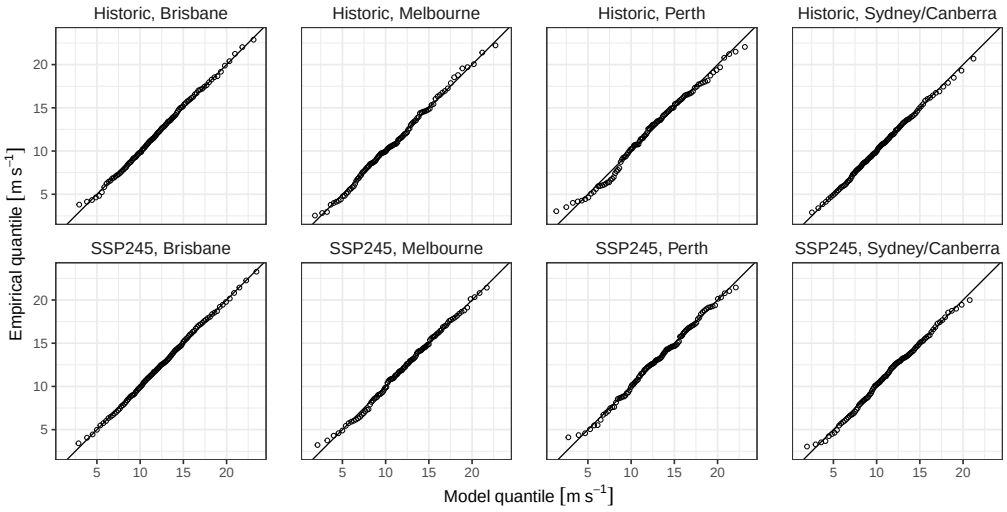

Figure 5. Quantile-quantile plots for GEV models fitted to daily maximum 10 m wind collocated with hail.

4.3 Changes in hail size

Figure 8 shows return periods for maximum hail size. It is not uncommon for return period models based on the GEV family to produce non-physical extreme values such as the extremely large hail sizes predicted for large return periods here (Coles, 2001, p. 66). We take the advice of Coles (2001) and interpret the results here based on the shorter return periods, thus keeping physical principles in mind. In the two domains with significant changes there are increases in the maximum expected hail size for return periods out to about 30 hail days. Figure 8 also shows the probability of a hail day producing severe (20 mm), giant (50 mm), and 100 mm hail, respectively. In the Melbourne domain, the probability of a hail day producing severe hail jumps from 46% to 60%, the probability of a hail day producing giant hail more than doubles from 5% to 13%, and the probability of a hail day producing 100 mm hail triples from 1% to 4%. In the Sydney/Canberra domain,

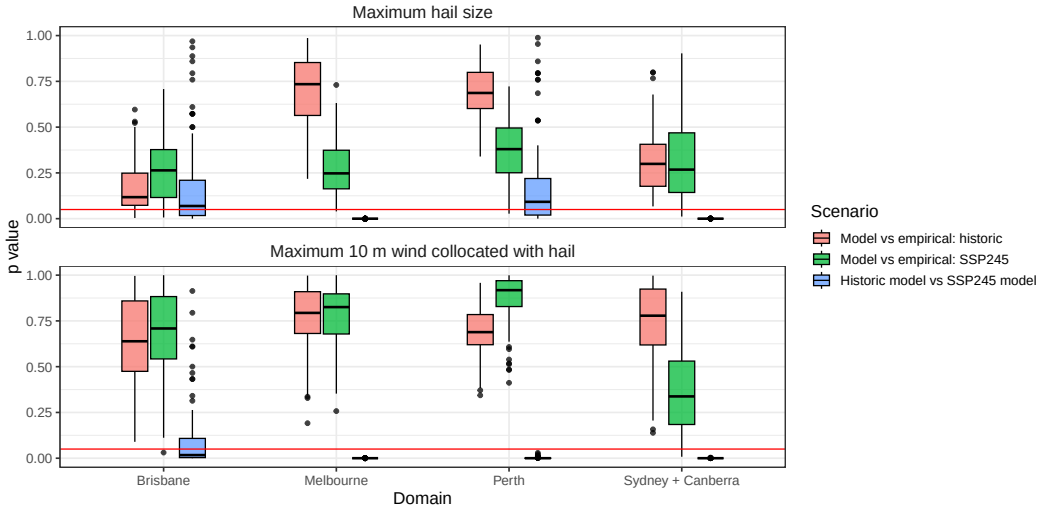

Figure 6. Distributions of p values from KS tests, comparing empirical values GEV models, and historical GEVs SSP245 GEVs, per variable and domain. For each test, the KS test was applied 100 times with 1000 random values drawn from the relevant GEV distribution(s) each time, to obtain a distribution of p values. Bars show medians, box hinges show the inter-quartile ranges (IQRs), whiskers show the largest (smallest) values no more than 1.5 × IQR from the upper (lower) hinge, and points show outlier points beyond the whisker ranges. The horizontal line shows $p = 0.05$; when p values are below this line the null hypothesis that the two samples come from the same distribution can be rejected.

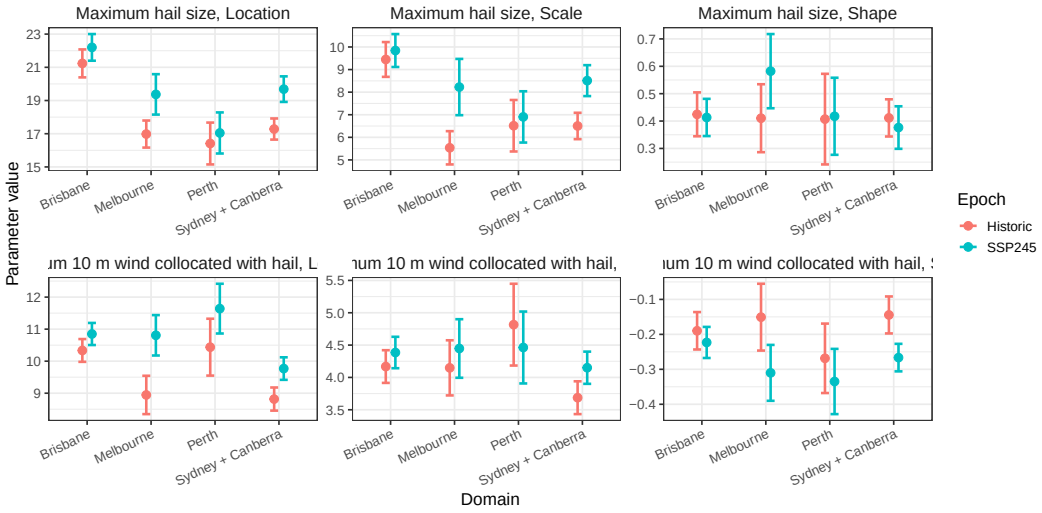

Figure 7. Location, scale, and shape parameter for fitted GEV distributions for maximum hail size (top row) and 10 m wind (bottom row). Parameter values are shown as a point; whiskers show 95% confidence intervals.

the probability of a hail day producing severe hail increases from 49% to 62%, while the probability of a hail day producing giant hail goes from 6% to 10% and the probability of a hail day producing 100 mm hail increases from 1% to 2%. The other two domains, in which the changes are not significant, show increases for severe hail but no changes in larger hail.

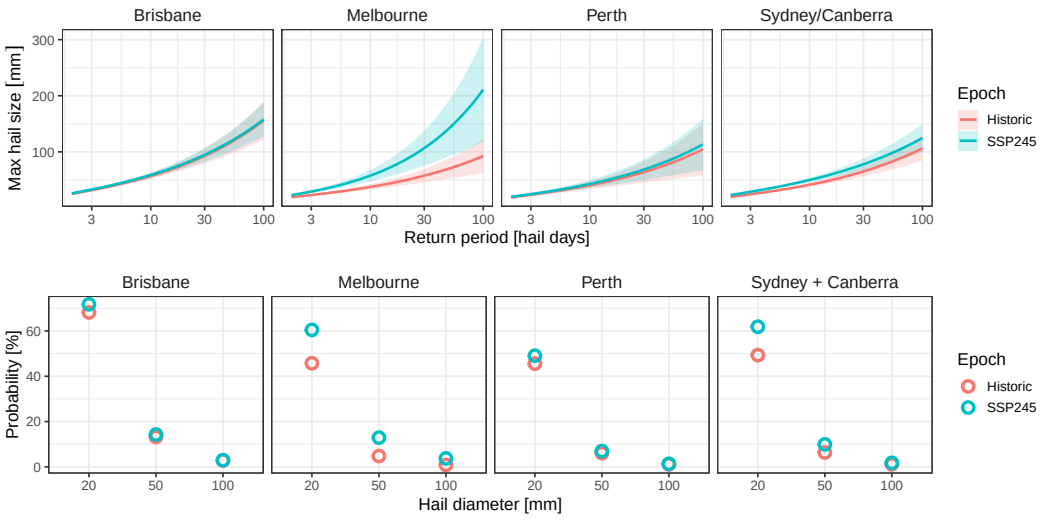

Figure 8. Return period plots by domain for maximum hail size (top row), and the probability of a hail day delivering severe (20 mm), giant (50 mm) and 100 mm hail by domain and epoch (bottom row).

4.4 Changes in 10 m wind at hail locations and times

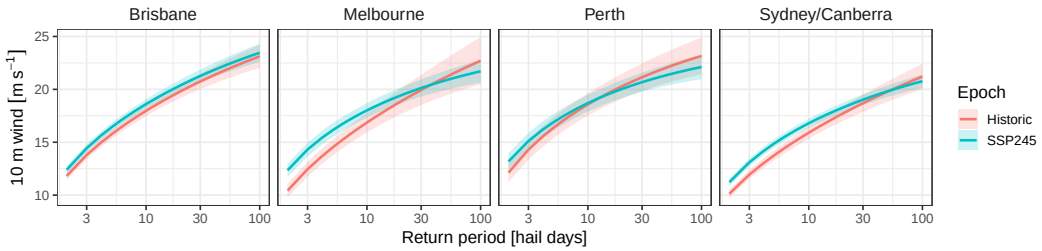

Figure 9. Return period plots by domain for 10 m wind collocated with hail.

Figure 9 shows return periods for 10 m wind collocated with hail. In Melbourne and Sydney/Canberra, the two domains with significant changes, there are increases in wind speeds for low return periods (up to 10 hail days), and decreases in wind speeds with very long return periods (50 to 100 hail days). We examined 100 km h^{-1} as a threshold for wind speeds that combined with hail can cause structural damage **(references)**. In both the Melbourne and Sydney/Canberra domains, the historical probability of a hail day producing a 100 km h^{-1} wind collocated with surface hail was very low (less than 0.1%) and the future probability is zero, according to the fitted GEVs. We note that extrapolating to very high levels in GEVs is discouraged (Coles, 2001), so these results must be intepreted with caution.

4.5 Changes in co-occurrence of hail and wind

- **(Caution that hail is max size per hour and wind is hourly instantaneous wind)**.

4.6 Changes in relevant atmospheric properties

- **(t test changes in CAPE, CIN, S06, etc.)**

5 Conclusions

Open Research Section

Boundary condition data are available at Xu et al. (2021a).

Acknowledgments

Since March 2024, THR's position at UNSW Sydney has been supported by QBE Insurance. This research was undertaken with the assistance of resources from the National Computational Infrastructure (NCI Australia), an NCRIS enabled capability supported by the Australian Government. We thank Simon Tett for useful discussions on extreme value techniques.

References

Adams-Selin, R. D., Clark, A. J., Melick, C. J., Dembek, S. R., Jirak, I. L., & Ziegler, C. L. (2019). Evolution of WRF-HAILCAST during the 2014–16 NOAA/Hazardous Weather Testbed spring forecasting experiments. *Weather Forecast*, *34*(1), 61-79. doi: 10.1175/waf-d-18-0024.1

Allen, J. T., Karoly, D. J., & Walsh, K. J. (2014). Future Australian severe thunderstorm environments. Part II: The influence of a strongly warming climate on convective environments. *J Climate*, *27*(10), 3848-3868. doi: 10.1175/JCLI-D-13-00426.1

Association of Consulting Structural Engineers. (2022). *Hail loading on roofs. Practice note number 19 version 2.* Retrieved from `https://www.acse.org.au/wp-content/uploads/2022/03/Practice-Paper-19-Hail-Loading-REVISED-2022.pdf` (accessed 22 June 2024)

Australian Building Codes Board. (2024). *National construction code.* Retrieved from `https://ncc.abcb.gov.au` (accessed 22 July 2024)

Bell, J. R., Wisinski, E. F., Molthan, A. L., Schultz, C. J., Gilligan, E., & Sharp, K. G. (2023). Developing a hail and wind damage swath event database from daily MODIS true color imagery and storm reports for impact analysis and applications. *Weather Forecast*, *38*(9), 1575 - 1588. doi: 10.1175/WAF-D-22-0210.1

Carletta, N. D. (2010). *Severe wind-driven hail events: Dependence on convective morphology and larger-scale environment* (Master's thesis, Department of Geological and Atmospheric Sciences. Iowa State University). Retrieved from `https://meteor.geol.iastate.edu/~ncarlett/portfolio/Senior_Thesis_Carletta_Final.pdf` (accessed 22 July 2024)

Changnon, S. A. (1967). Areal-temporal variations of hail intensity in Illinois. *J Appl Meteorol*, *6*(3), 536 - 541. doi: 10.1175/1520-0450(1967)006⟨0536:ATVOHI⟩2.0.CO;2

Coles, S. (2001). *An introduction to statistical modeling of extreme values* (1st ed.). Springer London. doi: 10.1007/978-1-4471-3675-0

Eyring, V., Bony, S., Meehl, G. A., Senior, C. A., Stevens, B., Stouffer, R. J., & Taylor, K. E. (2016). Overview of the Coupled Model Intercomparison Project Phase 6 (CMIP6) experimental design and organization. *Geosci Model Dev*, *9*(5), 1937–1958. doi: 10.5194/gmd-9-1937-2016

Gilleland, E., & Katz, R. W. (2016). extRemes 2.0: An extreme value analysis package in R. *J Stat Softw*, *72*(8), 1–39. doi: 10.18637/jss.v072.i08

Hersbach, H., Bell, B., Berrisford, P., Hirahara, S., Horányi, A., Muñoz Sabater, J., ... Thépaut, J.-N. (2020). The ERA5 global reanalysis. *Q J Roy Meteor Soc*, *146*(730),

1999-2049. doi: https://doi.org/10.1002/qj.3803

Hong, S.-Y., Noh, Y., & Dudhia, J. (2006). A new vertical diffusion package with an explicit treatment of entrainment processes. *Mon Weather Rev*, *134*(9), 2318 - 2341. doi: 10.1175/MWR3199.1

Iacono, M. J., Delamere, J. S., Mlawer, E. J., Shephard, M. W., Clough, S. A., & Collins, W. D. (2008). Radiative forcing by long-lived greenhouse gases: Calculations with the AER radiative transfer models. *J Geophys Res-Atmos*, *113*(D13). doi: 10.1029/2008JD009944

Institute for Catastrophic Loss Reduction. (2018). *Protect your home from hail.* Retrieved from `https://www.iclr.org/wp-content/uploads/2021/04/ICLR_Hail-2020_E_2021.pdf` (accessed 22 July 2024)

Insurance Council of Australia. (2024). *Historical normalised catastrophes, June 2024.* Retrieved from `https://insurancecouncil.com.au/wp-content/uploads/2024/07/ICA-Historical-Normalised-Catastrophe-June-2024.xlsx` (accessed 22 July 2024)

International Code Council. (2008). *International building code - structural.* Retrieved from `https://www.iccsafe.org/cs/codes/Documents/2007-08cycle/FAA/IBC-S1-S141-P2.pdf` (accessed 22 July 2024)

Jiménez, P. A., Dudhia, J., González-Rouco, J. F., Navarro, J., Montávez, J. P., & García-Bustamante, E. (2012). A revised scheme for the wrf surface layer formulation. *Mon Weather Rev*, *140*(3), 898 - 918. doi: 10.1175/MWR-D-11-00056.1

Milbrandt, J. A., Morrison, H., II, D. T. D., & Paukert, M. (2021). A triple-moment representation of ice in the predicted particle properties (P3) microphysics scheme. *J Atmos Sci*, *78*(2), 439 - 458. doi: 10.1175/JAS-D-20-0084.1

Niu, G.-Y., Yang, Z.-L., Mitchell, K. E., Chen, F., Ek, M. B., Barlage, M., ... Xia, Y. (2011). The community Noah land surface model with multiparameterization options (Noah-MP): 1. model description and evaluation with local-scale measurements. *J Geophys Res-Atmos*, *116*(D12). doi: 10.1029/2010JD015139

O'Neill, B. C., Kriegler, E., Ebi, K. L., Kemp-Benedict, E., Riahi, K., Rothman, D. S., ... Solecki, W. (2017). The roads ahead: Narratives for shared socioeconomic pathways describing world futures in the 21st century. *Glob Environ Change*, *42*, 169-180. doi: 10.1016/j.gloenvcha.2015.01.004

R Core Team. (2023). R: A language and environment for statistical computing [Computer software manual]. Vienna, Austria. Retrieved from `https://www.R-project.org/`

Skamarock, W. C., Klemp, J. B., Dudhia, J., Gill, D. O., Liu, Z., Berner, J., ... yu Huang, X. (2021, 7 20). *A description of the advanced research WRF version 4.3* (Tech. Rep.). Boulder, Colorado, USA: National Center for Atmospheric Research. (NCAR technical note NCAR/TN-556+STR) doi: 10.5065/1dfh-6p97

Standards Australia. (2021). *AS/NZS 1170.2 structural design actions, part 2 wind actions.* Retrieved from `https://store.standards.org.au/product/as-nzs-1170-2-2021` (accessed 22 July 2024)

Towery, N. G., Morgan, G. M., & Changnon, S. A. (1976). Examples of the wind factor in crop-hail damage. *J Appl Meteorol*, *15*(10), 1116 - 1120. doi: 10.1175/1520-0450(1976)015⟨1116:EOTWFI⟩2.0.CO;2

Walsh, K., White, C. J., McInnes, K., Holmes, J., Schuster, S., Richter, H., ... Warren, R. A. (2016). Natural hazards in Australia: storms, wind and hail. *Climatic Change*, *139*(1), 55-67. doi: 10.1007/s10584-016-1737-7

Xu, Z., Han, Y., Tam, C.-Y., Yang, Z.-L., & Fu, C. (2021a, January). *Bias-corrected CMIP6 global dataset for dynamical downscaling of the Earth's historical and future climate (1979-2100).* Science Data Bank. doi: 10.11922/sciencedb.00487

Xu, Z., Han, Y., Tam, C.-Y., Yang, Z.-L., & Fu, C. (2021b). Bias-corrected cmip6 global dataset for dynamical downscaling of the historical and future climate (1979–2100). *Sci Data*, *8*(1), 293. doi: 10.1038/s41597-021-01079-3

Zhang, C., & Wang, Y. (2017). Projected future changes of tropical cyclone activity over the Western North and South Pacific in a 20-km-mesh regional climate model. *J Climate*,

295 *30*(15), 5923 - 5941. doi: 10.1175/JCLI-D-16-0597.1

Appendix

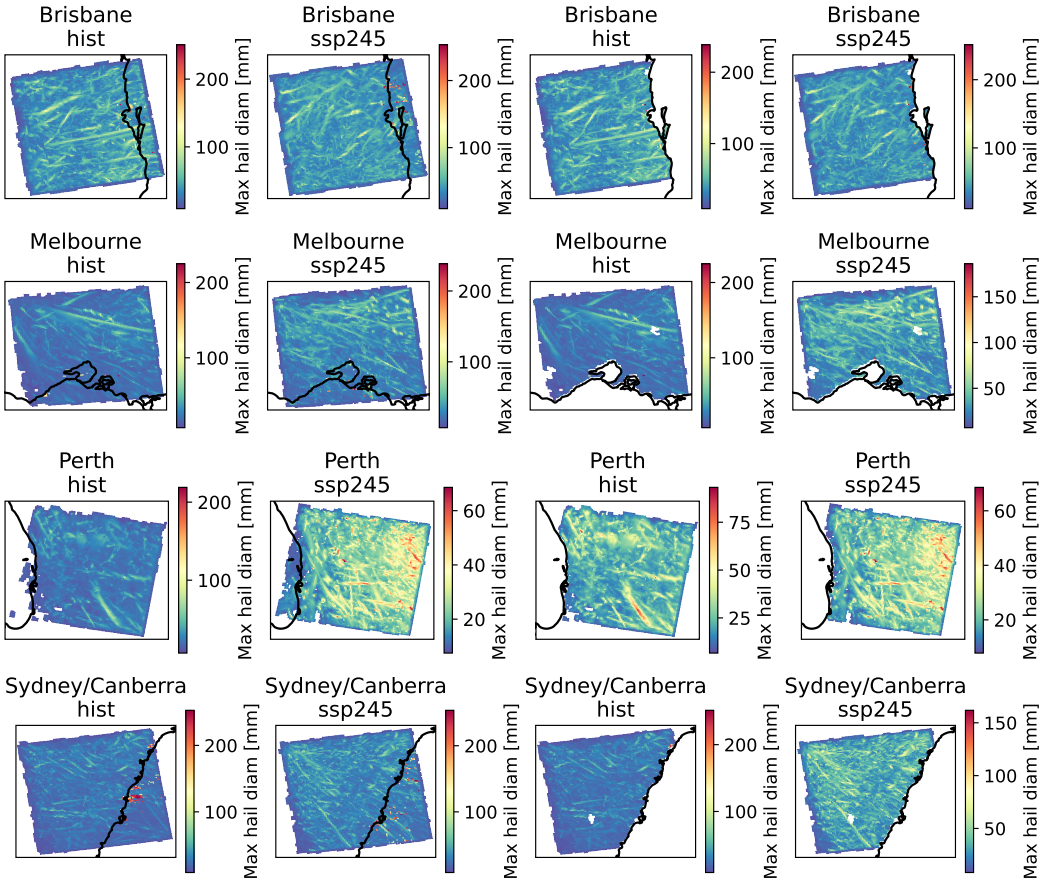

Figure A1. Maximum hail size diameters for the Brisbane, Melbourne, Perth, and Sydney/Canberra domains under the historical (hist) and future (ssp245) scenarios, with and without ocean areas removed.